The Cryosphere

EGU

Open Access

Supplement of

Effects of Arctic sea-ice concentration on surface radiative fluxes in four atmospheric reanalyses

Tereza Uhlíková et al.

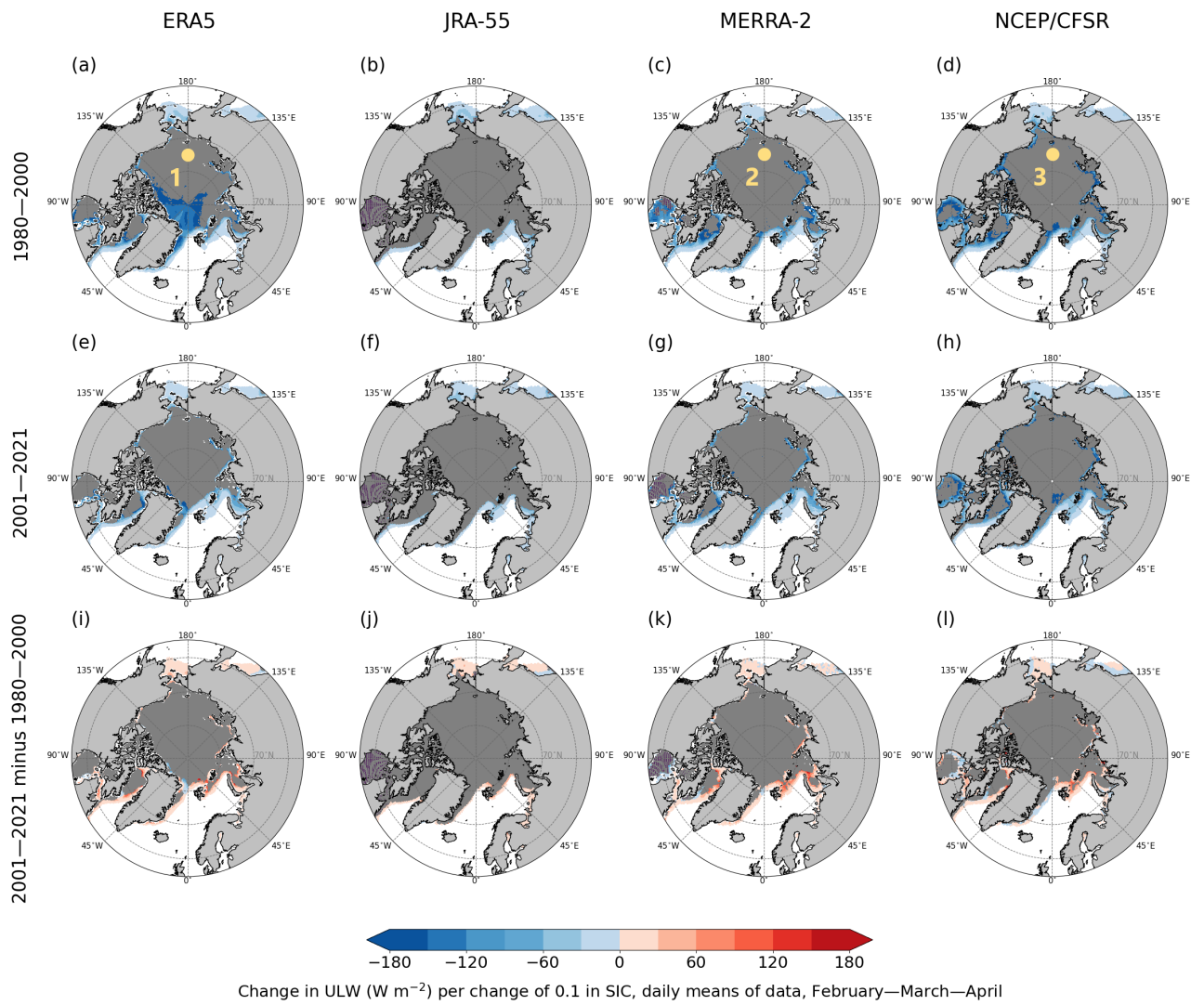*Correspondence to:* Tereza Uhlíková (tereza.uhlikova@helsinki.fi)

Figure S 1: Change in upward longwave radiative flux (W m^{-2}) per 0.1 change in sea-ice concentration (slope of regression line) in the marine Arctic in February–March–April in four reanalyses (columns), based on the linear orthogonal distance regression (ODR) model. Dark grey indicates areas where the ODR model did not converge; in panels **(i)**−**(l)**, dark grey shows these areas in 1980–2000 and/or 2001–2021. Only grid cells with a mean of SIC > 0.5 were considered, and only the slopes whose 95 % confidence intervals do not overlap zero are shown (others are masked in white). Points 1, 2, 3 (in yellow) from panels **(a), (c), (d)** are further analysed in Figure S2.
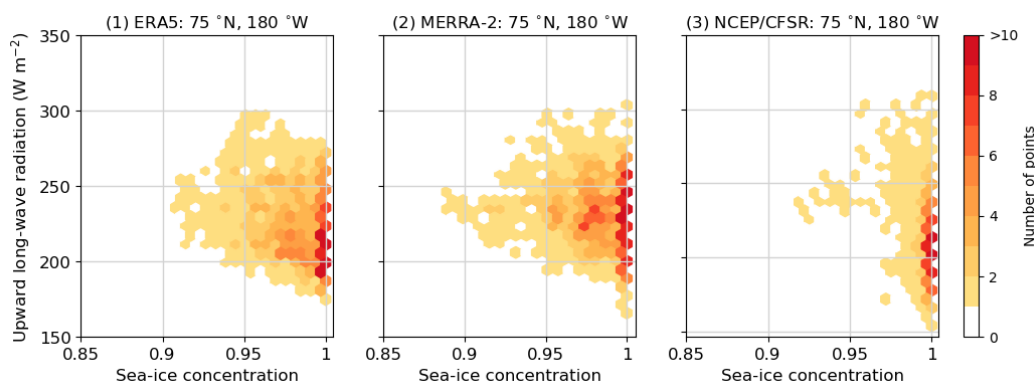

Figure S 2: Daily sea-ice concentration and upward longwave radiative flux in selected grid cells on the border of Chukchi and East Siberian seas, where the orthogonal distance regression model did not converge. Data from ERA5 **(1)**, MERRA-2 **(2)**, and NCEP/CFSR **(3)** (as indicated in Figure S1 in panels **(a), (c), (d)**) show days in February–March–April 1980–2000 (1875 d) in grid cells nearest to 75° N, 180° E.
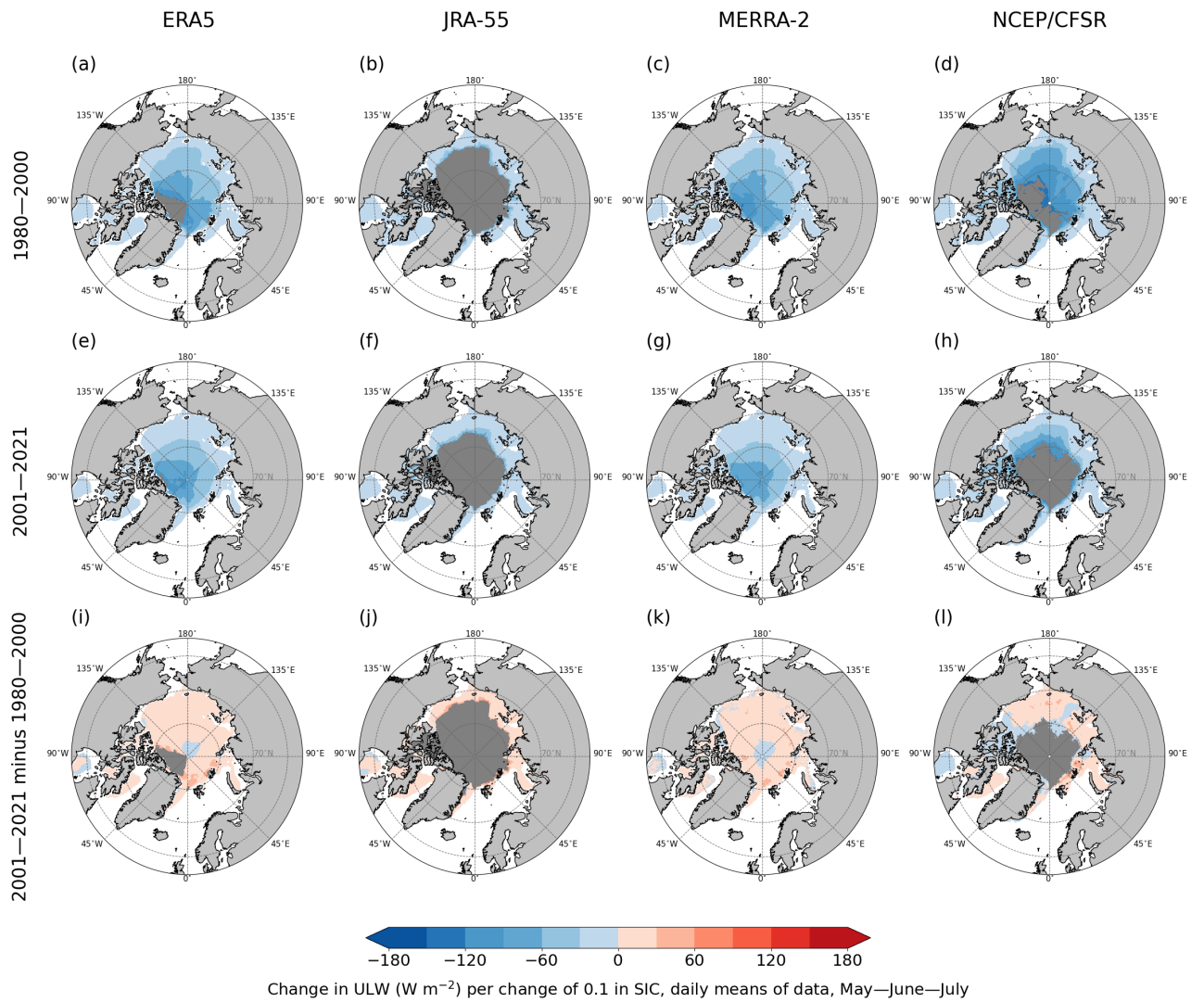
Figure S 3: Change in upward longwave radiative flux (W m^{-2}) per 0.1 change in sea-ice concentration (slope of regression line) in the marine Arctic in May–June–July in four reanalyses (columns), based on the linear orthogonal distance regression (ODR) model. Dark grey indicates areas where the ODR model did not converge; in panels **(i)−(l)**, dark grey shows these areas in 1980–2000 and/or 2001–2021. Only grid cells with a mean of SIC > 0.5 were considered, and only the slopes whose 95 % confidence intervals do not overlap zero are shown (others are masked in white).
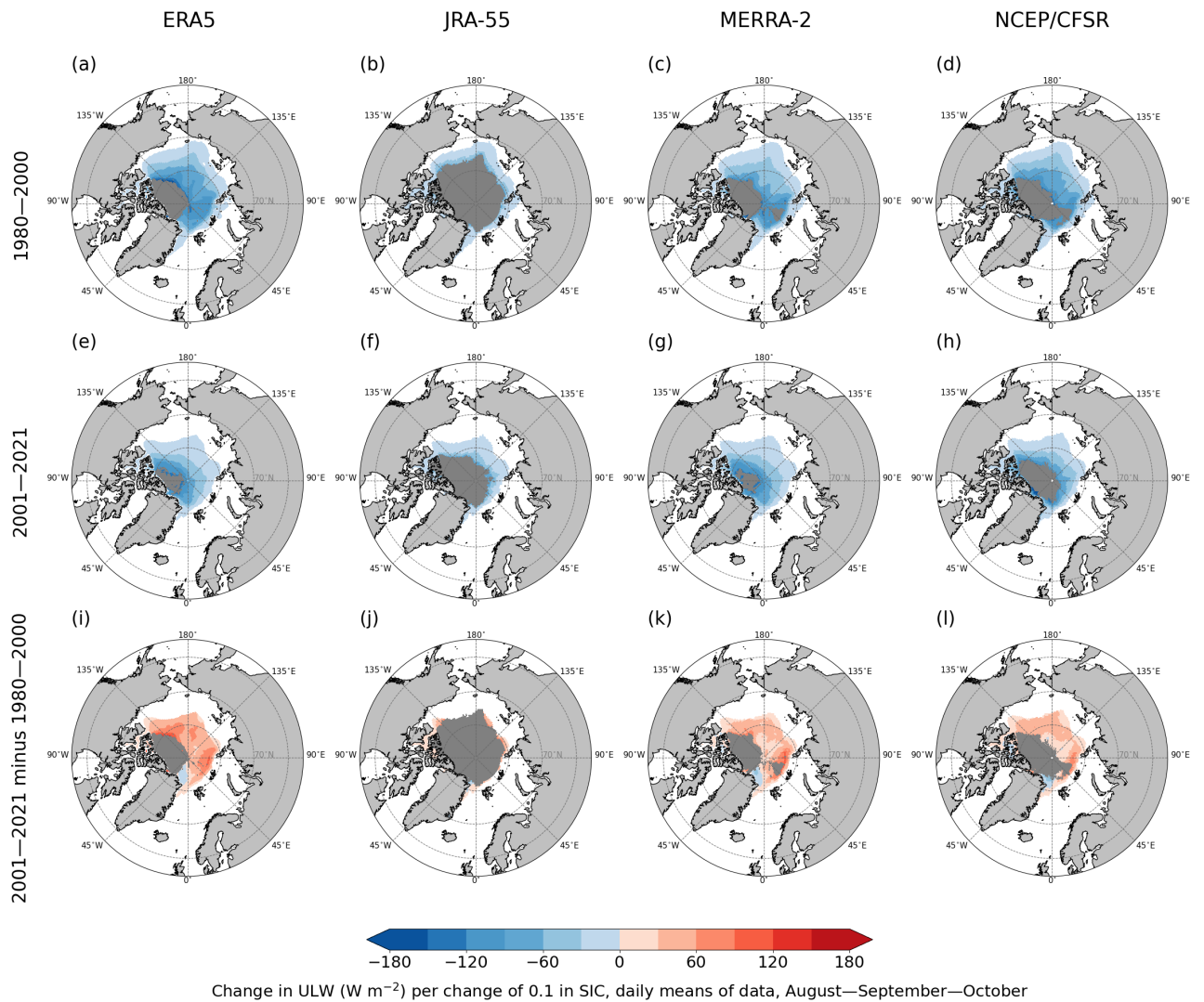
Figure S 4: Change in upward longwave radiative flux (W m^{-2}) per change of 0.1 in sea-ice concentration (slope of regression line) in the marine Arctic in August–September–October in four reanalyses (columns), based on the linear orthogonal distance regression (ODR) model. Dark grey indicates areas where the ODR model did not converge; in panels **(i)**–**(l)**, dark grey shows these areas in 1980–2000 and/or 2001–2021. Only grid cells with a mean of SIC > 0.5 were considered, and only the slopes whose 95 % confidence intervals do not overlap zero are shown (others are masked in white).
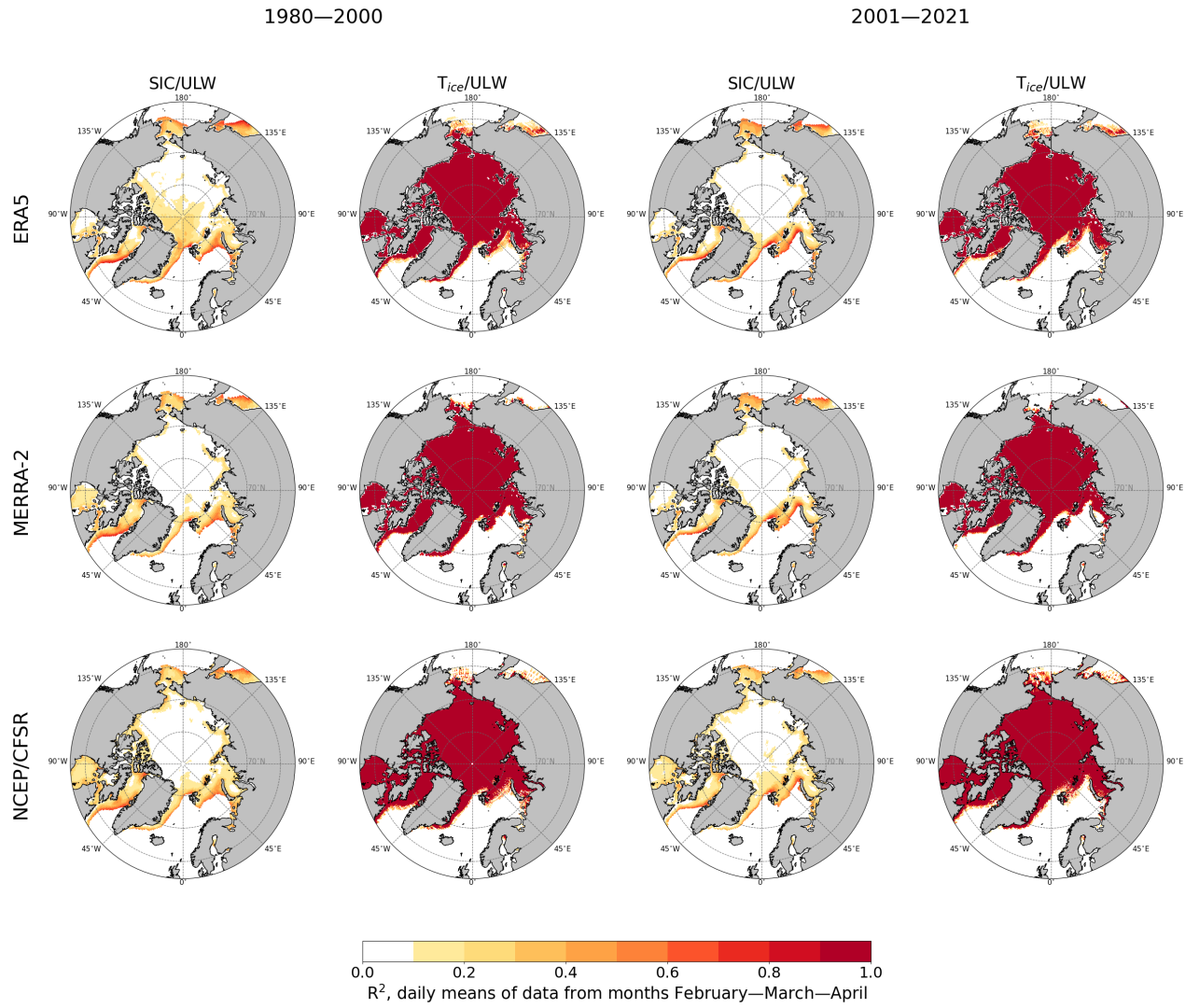
Figure S 5: Proportion of variance in the upward longwave radiation (ULW) explained by sea-ice concentration (SIC) and surface temperature of the ice (T_{ice}) in February–March–April in 1980–2000 and 2001–2021 (columns), as represented in three reanalyses (rows), based on the linear ordinary least square regression model (coefficient of determination, R^2) using daily means of data from ERA5, MERRA-2, and NCEP/CFSR. Only grid cells with a mean of SIC > 0.5 were considered and only statistically significant results at the 5 % level of significance are shown (insignificant values are masked in white).
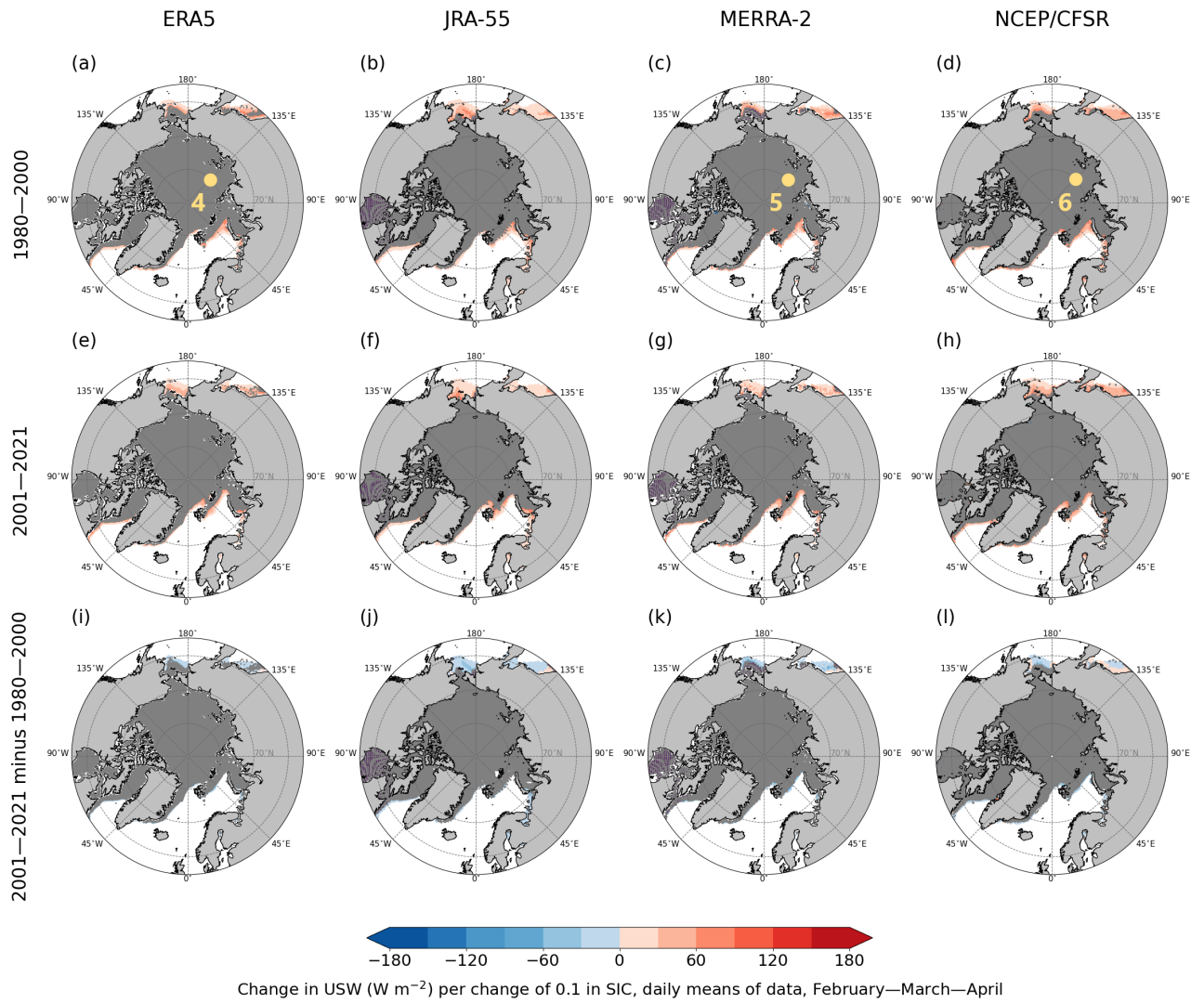
ERA5   JRA-55   MERRA-2   NCEP/CFSR

1980—2000

(a)   (b)   (c)   (d)

2001—2021

(e)   (f)   (g)   (h)

2001—2021 minus 1980—2000

(i)   (j)   (k)   (l)

Change in USW (W m^{-2}) per change of 0.1 in SIC, daily means of data, February—March—April

Figure S 6: Change in upward shortwave radiative flux (W m^{-2}) per 0.1 change in sea-ice concentration (slope of regression line) in the marine Arctic in February–March–April in four reanalyses (columns), based on the linear orthogonal distance regression (ODR) model. Dark grey indicates areas where the ODR model did not converge; in panels **(i)–(l)**, dark grey shows these areas in 1980–2000 and/or 2001–2021. Only grid cells with a mean of SIC > 0.5 were considered, and only the slopes whose 95 % confidence intervals do not overlap zero are shown (others are masked in white). Points 4, 5, 6 (in yellow) from panels **(a), (c), (d)** are further analysed in Figure S7.
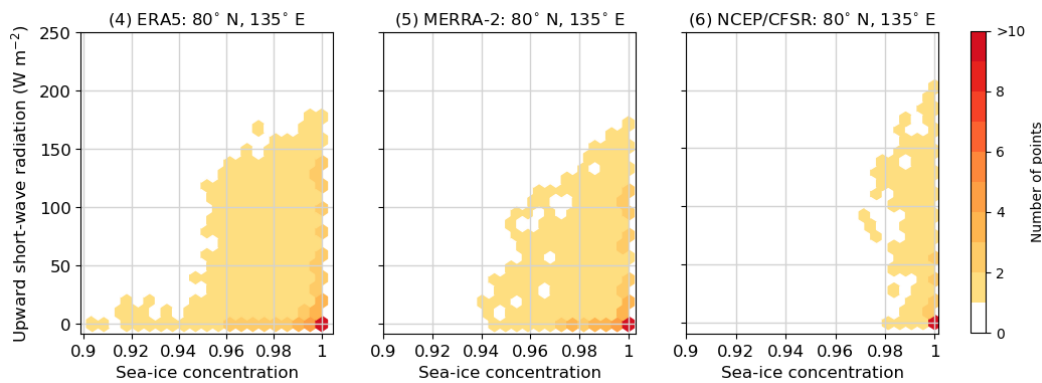

Figure S 7: Daily sea-ice concentration and upward shortwave radiative flux in selected grid cells in the Laptev Sea, where the orthogonal distance regression model did not converge. Data from ERA5 **(4)**, MERRA-2 **(5)**, and NCEP/CFSR **(6)** (as indicated in Figure S6 in panels **(a), (c), (d)**) show days in February–March–April 1980–2000 (1875 d) in grid cells nearest to 80° N, 135° E.
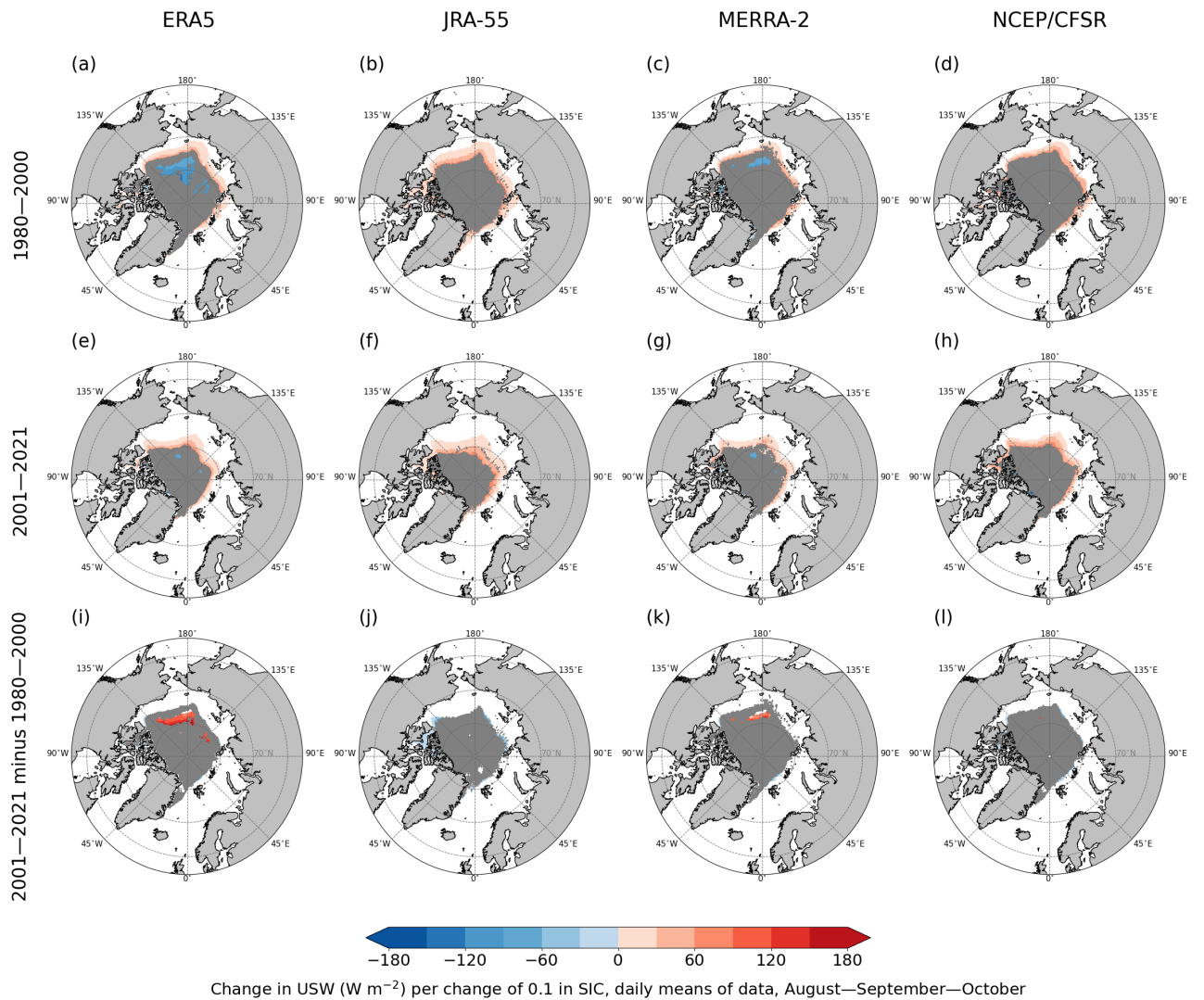
5

Figure S 8: Change in upward shortwave radiative flux (W m^{-2}) per 0.1 change in sea-ice concentration (slope of regression line) in the marine Arctic in August–September–October in four reanalyses (columns), based on the linear orthogonal distance regression (ODR) model. Dark grey indicates areas where the ODR model did not converge; in panels **(i)−(l)**, dark grey shows these areas in 1980–2000 and/or 2001–2021. Only grid cells with a mean of SIC > 0.5 were considered, and only the slopes whose 95 % confidence intervals do not overlap zero are shown (others are masked in white).
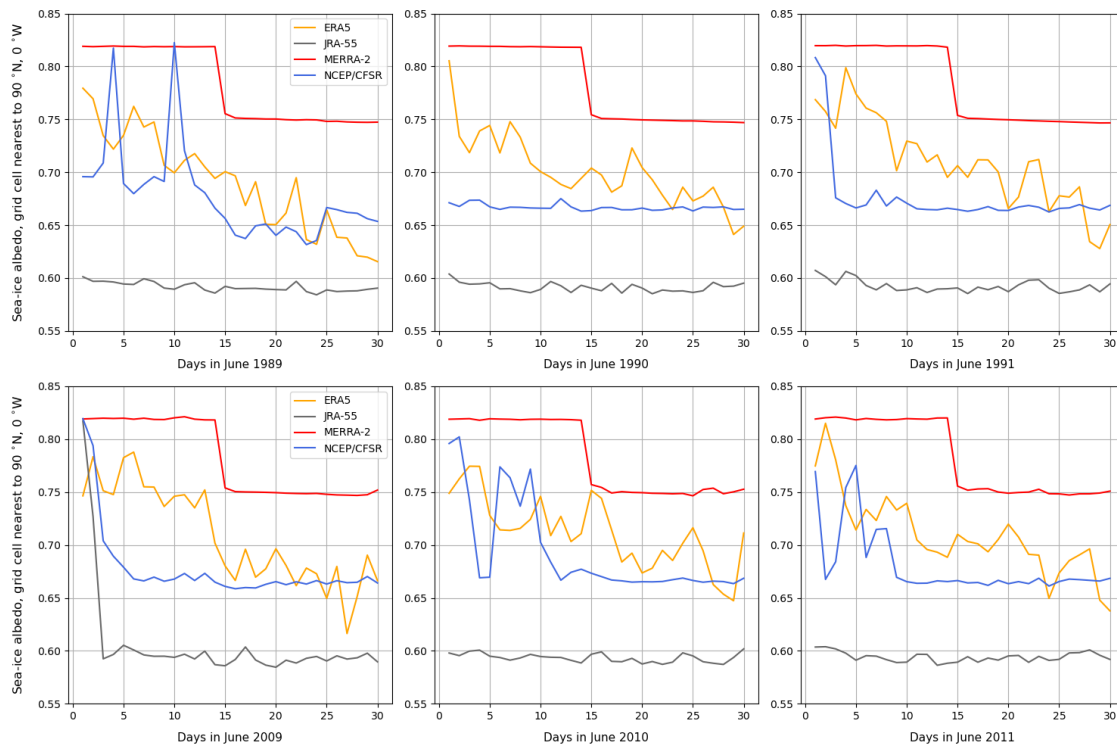
Figure S 9: Daily sea-ice albedo in the grid cell nearest to the North Pole (90° N, 0° W) in four reanalyses. Three Junes in the middle of the first study period (1989, 1990, 1991) and three Junes in the middle of the second study period (2009, 2010, 2011).
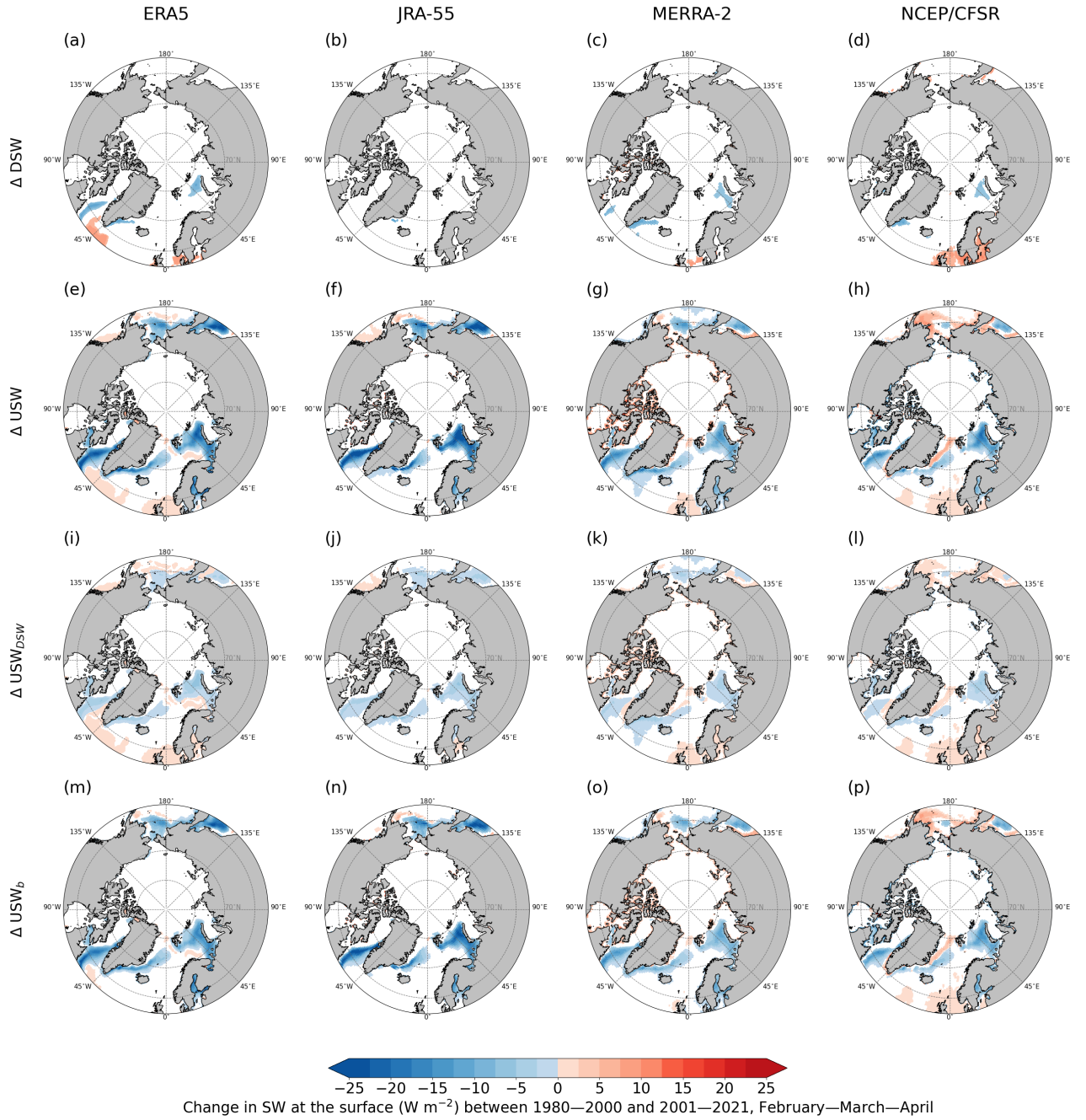
Figure S 10: Changes in decadal means (calculated from daily means) between 1980–2000 and 2001–2021 in February–March–April. Panels **(a)**–**(h)** show changes in surface downward and upward shortwave radiative fluxes (ΔDSW; ΔUSW), panels **(i)**–**(l)** show changes in USW explained by changes in DSW (Δ USW$_{DSW}$), and panels **(m)**–**(p)** show changes in USW explained by changes in albedo (Δ USW$_{b}$). Only statistically significant results at the 5 % level of significance are shown (insignificant values are masked in white); statistically significant grid cells for ΔUSW, Δ USW$_{DSW}$, and Δ USW$_{b}$ are identical. Values within an interval (-0.1,0.1) W m^{-2} are also masked in white.
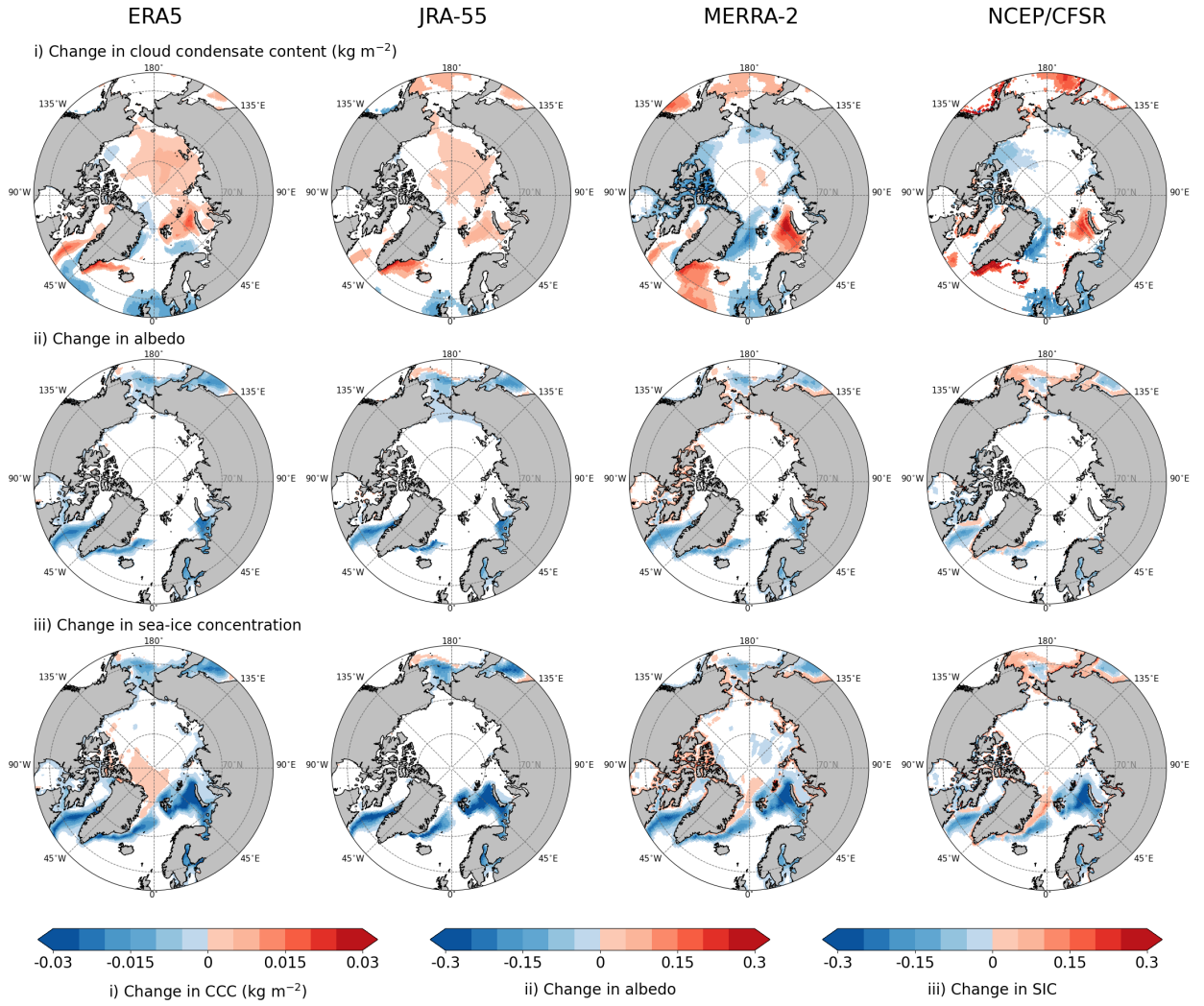
Figure S 11: Changes in decadal means (calculated from daily means) for 2001–2021 minus 1980–2000 in February–March–April. Row **(i)** shows the cloud condensate content (CCC, vertically integrated cloud liquid water + ice), row **(ii)** shows the surface albedo, and row **(iii)** shows the sea-ice concentration (SIC). Only statistically significant results at the 5 % level of significance are shown (insignificant values are masked in white). In rows **(ii)** and **(iii)**, values within an interval (-0.01,0.01) are also masked in white.
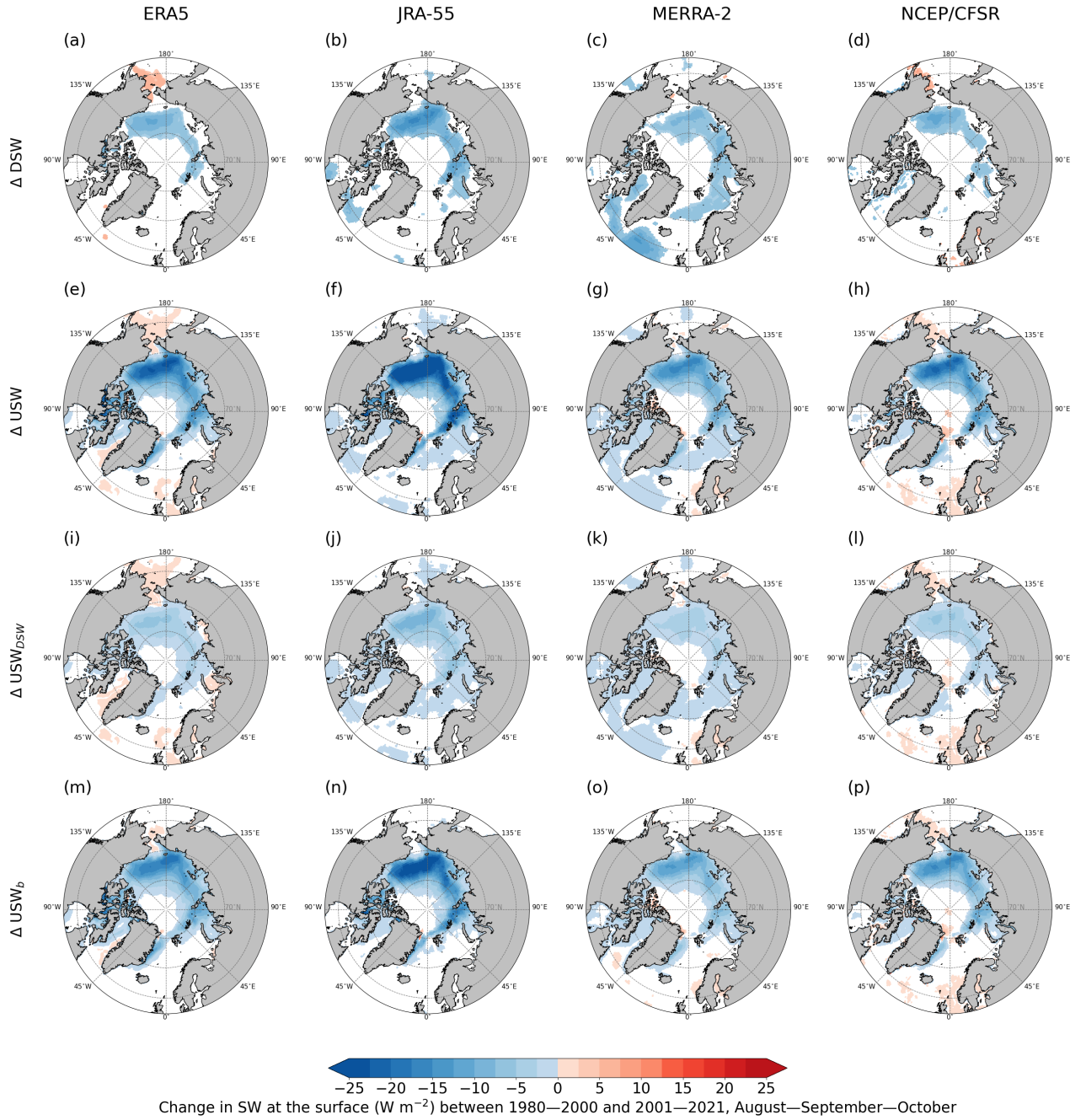
Figure S 12: Changes in decadal means (calculated from daily means) between 1980–2000 and 2001–2021 in August–September–October. Panels **(a)–(h)** show changes in surface downward and upward shortwave radiative fluxes (ΔDSW; ΔUSW), panels **(i)–(l)** show changes in USW explained by changes in DSW (Δ USW$_{\text{DSW}}$), and panels **(m)–(p)** show changes in USW explained by changes in albedo (Δ USW$_{\text{b}}$). Only statistically significant results at the 5 % level of significance are shown (insignificant values are masked in white); statistically significant grid cells for ΔUSW, Δ USW$_{\text{DSW}}$, and Δ USW$_{\text{b}}$ are identical. Values within an interval (-0.1,0.1) W m^{-2} are also masked in white.
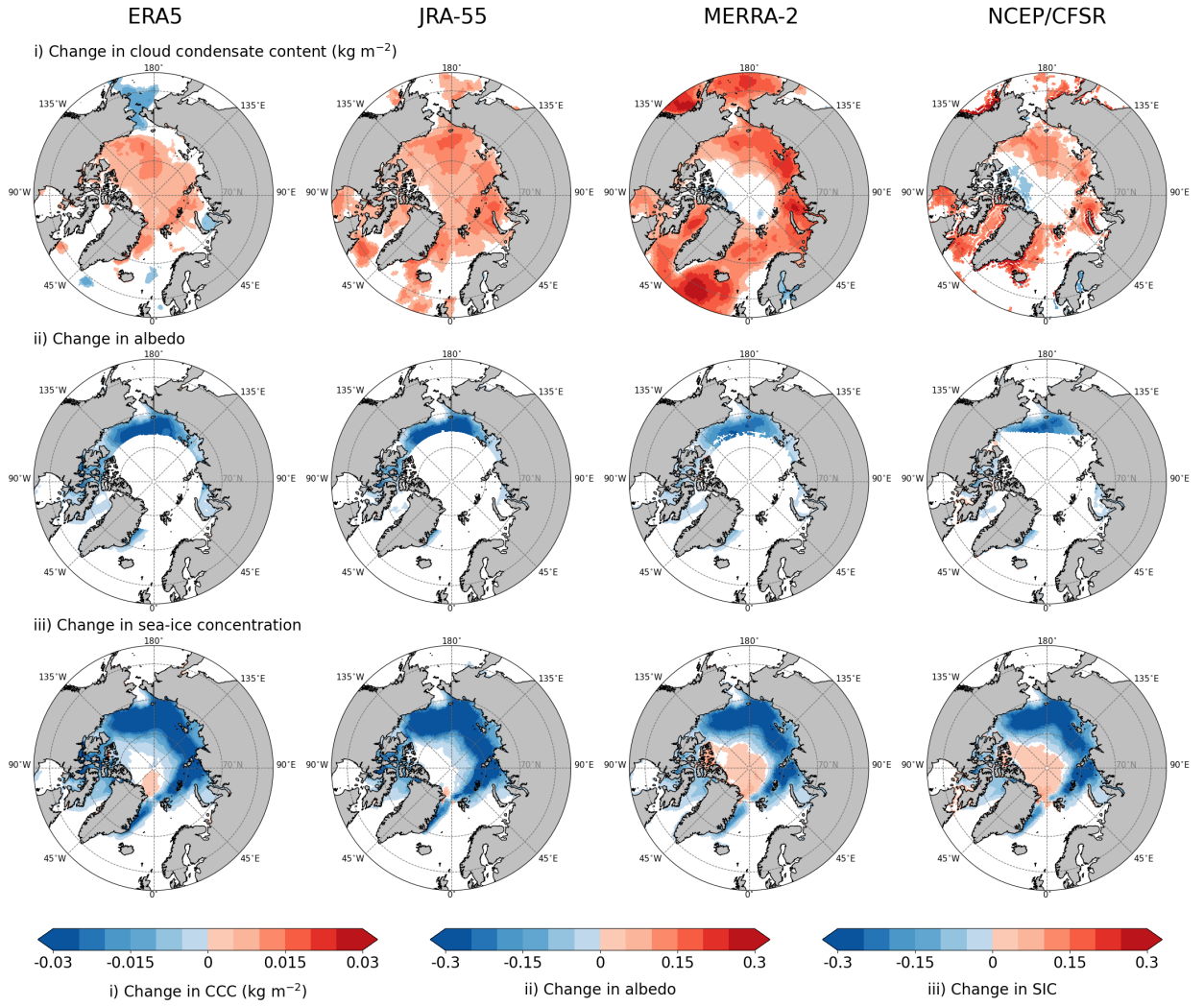
Figure S 13: Changes in decadal means (calculated from daily means) for 2001–2021 minus 1980–2000 in August–September–October. Row **(i)** shows the cloud condensate content (CCC, vertically integrated cloud liquid water + ice), row **(ii)** shows the surface albedo, and row **(iii)** shows the sea-ice concentration (SIC). Only statistically significant results at the 5 % level of significance are shown (insignificant values are masked in white). In rows **(ii)** and **(iii)**, values within an interval (-0.01,0.01) are also masked in white.